Harmonic Current Controller Design for Anisotropic Synchronous Machines based on a Machine Model in Harmonic Reference Frame

A. Haspel[1], K. Kaiser[1], V. Ketchedjian[1] and J. Roth-Stielow[1]
[1] Institute for Power Electronics and Electrical Drives, University of Stuttgart, Germany

***Abstract*-- This paper proposes a novel controller design for harmonic current control of synchronous machines based on a plant model in a harmonic reference frame. The modeling in the harmonic reference frame exposes additional harmonic couplings in the plant's transfer function, caused by the different inductances in the direct- and quadrature-axis of the rotor. These effects disturb conventional harmonic controllers. Therefore, the proposed controller uses an inverse plant model including the additional harmonic couplings, to achieve the desired stationary and dynamic behavior. The implementation of the novel harmonic controller, simulations and experimental results are presented for a permanent magnet assisted synchronous reluctance machine.**

***Index Terms*—Controller design, harmonic current control, harmonic reference frame, synchronous machine.**

I. Introduction

There are various causes for harmonics in the flux or currents of electric machines. The order and the magnitude of the harmonics strongly depend on the design of the machine, in particular the geometry of the magnetic iron, the winding scheme and the permanent magnet (PM) flux distribution [1]. Since harmonics usually create additional losses and can lead to vibrations, current control systems generally aim to eliminate harmonics to achieve pure sinusoidal current waveforms. However, [1], [2] and [3] state that the current waveforms of synchronous machines should be adapted to the waveforms of the back-EMF to minimize the torque pulsation. Therefore, an additional injection of specific current harmonics can be required. The injection of harmonics can further be used for active noise cancelation.

Both elimination and injection of harmonics require a precise control system. Within the established stator fixed (αβ) reference frame or the rotor-flux oriented (dq) reference frame, harmonics appear as time variant disturbances that challenge the control system, especially for higher speed. A transformation into a rotating reference system, similar to the one used for field-oriented control, allows the modeling of individual harmonics as DC-signals and therewith an easier control. [4] and [5] propose a control system in those harmonic reference frames (HRFs) but use simplified controller structures neglecting the anisotropic influence. While [4] considers only harmonics of the PM-flux, the machine model proposed in this paper focuses on the flux caused by the stator currents, which is dominant in permanent magnet assisted synchronous reluctance machines (PMaSynRMs). The machine model in these HRFs, which is introduced in section II of this paper, points out that an excitation of the machine with a specific harmonic will lead to a system response with the same harmonic order of the excitation and a second harmonic frequency, if the machine is anisotropic.

To achieve a suitable control over this plant behavior, a novel controller structure based on the inverse plant model is proposed in section III. [6] also defines an inverse plant based controller and compares its dynamic performance and robustness to those of other harmonic controller approaches. In comparison to this work, the inverse plant based controller in [6] is implemented as resonant controller in the fundamental dq-reference frame. It is further denoted by RINV. The implementation of the inverse controller in the HRFs, as proposed in this paper, provides a higher degree of freedom and can reduce dynamic control errors compared to the RINV.

Section IV presents a simulative examination of the proposed controller design. The elimination of harmonics in the stator currents is tested on a machine model with rotor angle and current dependent parameters. Moreover, the precise injection of selective harmonics that follows a desired dynamic behavior with zero steady-state deviation from the reference is demonstrated and compared to the behavior of the RINV. The presentation of measurement results in section V further validates the control quality and the robustness of the novel harmonic current controller for different operating points. An upper speed limit for the correct operation of the controllers is discussed as well.

II. Modeling of Anisotropic Synchronous Machines in Harmonic Reference Frames

With respect to the αβ-reference frame, the HRFs regarded in this paper rotate with integer multiples of the fundamental electric angular speed ω, according to the order of the harmonic x. The relevant harmonic orders in the αβ-reference frame are given by $x = 6n+1$. Positive values of the integer n imply that the HRF is rotating in the direction of the field-oriented reference frame. Negative values lead to a HRF rotating in the opposite direction. Regarded in the dq-reference frame, the effective order of the harmonics is shifted by one. Therefore, the 7^{th} and -5^{th} harmonic orders in the αβ-reference frame appear as $\pm 6^{th}$ harmonic orders in the dq-reference frame.

In order to design a suitable control system, the transfer characteristic of the plant should be well-known in the relevant reference frame. In the dq-reference frame, the transfer characteristic of a synchronous machine is given by the voltage equation (1) with the flux definition (2).

$$\underline{v}^{\mathrm{dq}} = R \cdot \underline{i}^{\mathrm{dq}} + \frac{\mathrm{d}\,\underline{\Psi}^{\mathrm{dq}}}{\mathrm{d}t} + \omega \cdot \begin{bmatrix} 0 & -1 \\ 1 & 0 \end{bmatrix} \cdot \underline{\Psi}^{\mathrm{dq}} \tag{1}$$

$$\underline{\Psi}^{\mathrm{dq}} = \begin{bmatrix} L_{\mathrm{d}} & 0 \\ 0 & L_{\mathrm{q}} \end{bmatrix} \cdot \underline{i}^{\mathrm{dq}} + \begin{bmatrix} \Psi_{\mathrm{PM}} \\ 0 \end{bmatrix} \tag{2}$$

The vectors $\underline{v}, \underline{i}, \underline{\Psi}$ denote the voltage, the current and the flux and can also be interpreted as complex numbers, where the first vector element describes the real part and the second element the imaginary part. R denotes the ohmic stator winding resistance, Ψ_{PM} represents the PM-flux and L_{d}, L_{q} denote the direct and quadrature inductances. The superscript 'dq' expresses that the vectors are described in the dq-reference frame. Since the PM-flux is assumed to be independent from the current in the machine, it is regarded as a disturbance for the further calculation. To describe the plant behavior in the HRFs, the voltage, current and flux vectors are rotated by the matrix (3), where φ_{e} denotes the angle between the αβ- and the dq-reference frame. $\underline{f}$ denotes any regarded vector, the superscript 'hx' describes that the vector refers to the HRF of the harmonic order x. The direct and quadrature elements of any vector in the hx-system are marked with the subscripts 'd' and 'q'.

$$\underline{f}^{\mathrm{h}x} = \begin{bmatrix} f_{\mathrm{d}}^{\mathrm{h}x} \\ f_{\mathrm{q}}^{\mathrm{h}x} \end{bmatrix} = \begin{bmatrix} \cos(6n\varphi_{\mathrm{e}}) & \sin(6n\varphi_{\mathrm{e}}) \\ -\sin(6n\varphi_{\mathrm{e}}) & \cos(6n\varphi_{\mathrm{e}}) \end{bmatrix} \cdot \underline{f}^{\mathrm{dq}} \tag{3}$$

Since the HRF is rotating compared to the rotor axis, the relation between the currents and the flux (respectively the inductances) are angle- and therefore time-dependent, see Eq. (4). In order to describe the flux in a HRF, the variables L_{m} and L_{Δ} are introduced.

$$\underline{\Psi}^{\mathrm{h}x} = \begin{bmatrix} L_{\mathrm{m}} - L_{\Delta} \cdot \cos(12n\omega t) & L_{\Delta} \cdot \sin(12n\omega t) \\ L_{\Delta} \cdot \sin(12n\omega t) & L_{\mathrm{m}} + L_{\Delta} \cdot \cos(12n\omega t) \end{bmatrix} \cdot \underline{i}^{\mathrm{h}x} \tag{4}$$

$$\text{with} \qquad L_{\mathrm{m}} = \frac{L_{\mathrm{d}} + L_{\mathrm{q}}}{2}, \qquad L_{\Delta} = \frac{L_{\mathrm{q}} - L_{\mathrm{d}}}{2}$$

Based on Eq. (4) and its derivation, the voltage equation in the HRF can be written as Eq. (5). The time-dependent elements of Eq. (4) are isolated and can be described by a time-dependent rotation, which can also be expressed as multiplication with a complex exponential function. The imaginary unit is denoted by j. The rotation indicates the introduction of additional frequency components. For $n = 0$ respectively $x = 1$ Eq. (5) simplifies to the voltage equation (1) in the fundamental dq-reference frame with neglected PM-flux. In the Laplace domain, the equation is given by (6), where s denotes the Laplace variable. The rotation in Eq. (5) results in a frequency shift from s to $s + j\omega 12n$ in the second summand of Eq. (6). Both Eqs. (5) and (6) point out that the time-dependent behavior respectively the additional frequency component in the plant's transfer function only appears if $L_{\Delta} \neq 0$.

A simulation clarifies the behavior more descriptively. The 7th voltage harmonic is applied on a standard model of an anisotropic synchronous machine with constant parameters and neglected PM-flux. The two upper plots in Fig. 1 show the applied voltage vector in two different reference frames, the stationary αβ-reference frame and the rotating h7-reference frame. In the two lower plots, the output current vector is given in the same reference frames. The applied 7th voltage harmonic of the αβ-system appears as DC-signal in the h7-system. According to the Eqs. (5) and (6), the output current of the machine shows the additional harmonic, which appears in the h7-system as -12th and in the αβ-system as -5th harmonics.

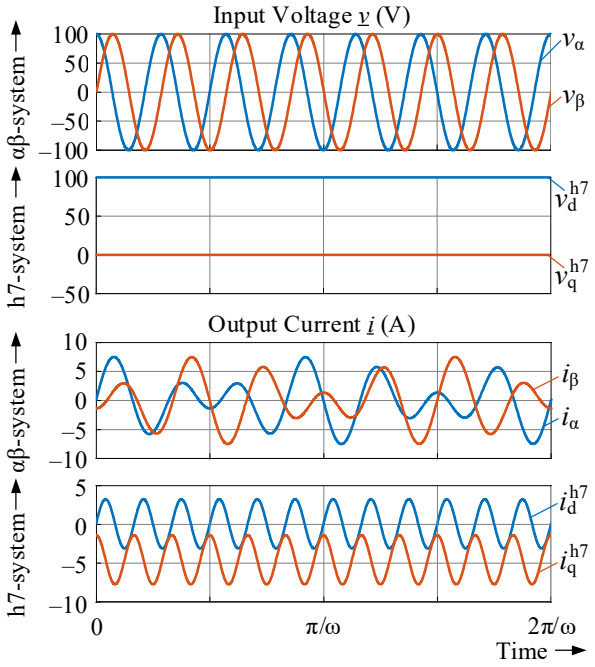

Fig. 1. Simulation of anisotropic machine with applied 7th voltage harmonic resulting in 7th and -5th current harmonics, shown in the stationary reference frame and the 7th HRF.

$$\underline{v}^{\mathrm{h}x} = \begin{bmatrix} R & -\omega(6n+1)L_{\mathrm{m}} \\ \omega(6n+1)L_{\mathrm{m}} & R \end{bmatrix} \cdot \underline{i}^{\mathrm{h}x} + \begin{bmatrix} L_{\mathrm{m}} & 0 \\ 0 & L_{\mathrm{m}} \end{bmatrix} \cdot \frac{\mathrm{d}\,\underline{i}^{\mathrm{h}x}}{\mathrm{d}t} + \underbrace{\begin{bmatrix} \cos(12n\omega t) & \sin(12n\omega t) \\ -\sin(12n\omega t) & \cos(12n\omega t) \end{bmatrix}}_{\triangleq e^{-j\omega 12nt}} \cdot \left(\begin{bmatrix} 0 & \omega(6n-1)L_{\Delta} \\ \omega(6n-1)L_{\Delta} & 0 \end{bmatrix} \cdot \underline{i}^{\mathrm{h}x} + \begin{bmatrix} -L_{\Delta} & 0 \\ 0 & L_{\Delta} \end{bmatrix} \cdot \frac{\mathrm{d}\,\underline{i}^{\mathrm{h}x}}{\mathrm{d}t} \right) \tag{5}$$

$$\underline{v}^{\mathrm{h}x}(s) = \begin{bmatrix} R + sL_{\mathrm{m}} & -\omega(6n+1)L_{\mathrm{m}} \\ \omega(6n+1)L_{\mathrm{m}} & R + sL_{\mathrm{m}} \end{bmatrix} \cdot \underline{i}^{\mathrm{h}x}(s) + \begin{bmatrix} -L_{\Delta}(s + j\omega 12n) & \omega(6n-1)L_{\Delta} \\ \omega(6n-1)L_{\Delta} & L_{\Delta}(s + j\omega 12n) \end{bmatrix} \cdot \underline{i}^{\mathrm{h}x}(s + j\omega 12n) \tag{6}$$

III. Controller Design

The harmonic controller proposed in the following subsection *A* controls only one specific harmonic. It is used as an extension of a fundamental controller implemented in the dq-reference frame, which is equal to the h1-reference frame. The structure can be implemented multiple times in parallel for all relevant harmonics, as described in subsection *B*.

A. Inverse plant based harmonic current controller

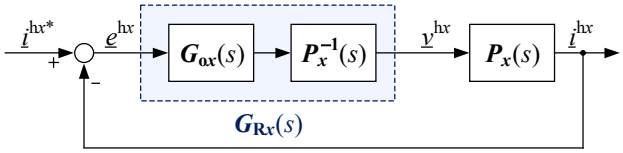

Fig. 2. Control loop schematic with inverse plant based controller.

The idea of an inverse plant based controller is illustrated in Fig. 2. $\underline{i}^{\mathrm{hx}*}$ denotes the setpoint values of the current vector in the h*x*-system. The transfer function of the controller $\boldsymbol{G}_{\mathbf{R}x}(s)$ is composed of two parts, the inverse plant model, denoted by $\boldsymbol{P}_x^{-1}(s)$, and the transfer function $\boldsymbol{G}_{\mathbf{0}x}(s)$. Since $\underline{v}^{\mathrm{hx}}(s) = \boldsymbol{P}_x^{-1}(s) \cdot \underline{i}^{\mathrm{hx}}(s)$, the inverse plant model in the x^{th} HRF is already given within Eq. (6). If the correct plant parameters are used in the inverse plant model, the inverse plant model within the controller compensates the transfer matrix of the real plant $\boldsymbol{P}_x(s)$. Hence, the selectable transfer function $\boldsymbol{G}_{\mathbf{0}x}(s)$ defines the open-loop transfer function of the control system. If the open-loop transfer function is implemented as diagonal integrator transfer matrix with selectable time-constants $T_{\mathrm{d}x}$ and $T_{\mathrm{q}x}$, the closed-loop transfer matrix is described with Eq. (7) and realizes the dynamic characteristic of decoupled PT1-elements with selectable time-constants $T_{\mathrm{d}x}$ and $T_{\mathrm{q}x}$.

$$\underline{i}^{\mathrm{hx}} = \begin{bmatrix} \dfrac{1}{1+sT_{\mathrm{d}x}} & 0 \\ 0 & \dfrac{1}{1+sT_{\mathrm{q}x}} \end{bmatrix} \cdot \underline{i}^{\mathrm{hx}*} \tag{7}$$

The combination of the open-loop transfer function with the transfer function of the inverse plant model results in the transfer matrix of the controller (8).

$$\boldsymbol{G}_{\mathbf{R}x}(s) = \boldsymbol{P}_x^{-1}(s) \cdot \boldsymbol{G}_{\mathbf{0}x}(s) = \boldsymbol{P}_x^{-1}(s) \cdot \begin{bmatrix} \dfrac{1}{sT_{\mathrm{d}x}} & 0 \\ 0 & \dfrac{1}{sT_{\mathrm{q}x}} \end{bmatrix} \tag{8}$$

Inserting Eq. (6) in Eq. (8) allows the calculation of the harmonic controller's output voltage, see Eq. (9), for the coefficients according to Eq. (10) below. The implementation for the x^{th} harmonic controller is illustrated in Fig. 3. The block $\boldsymbol{R}_{\boldsymbol{\alpha}}$ symbolizes a rotation matrix in Euclidean space with the rotating angle $\alpha = -12n \cdot \varphi_{\mathrm{e}}$.

B. Structure of the complete controller system

Figure 4 illustrates the combination of several harmonic controllers (HCs). In the presented example, the fundamental controller $\boldsymbol{G}_{\mathbf{R}1}(s)$ is extended by two HCs $\boldsymbol{G}_{\mathbf{R}7}(s)$ and $\boldsymbol{G}_{\mathbf{R}-5}(s)$. Each controller receives an individual setpoint current vector for the harmonic amplitudes but uses the overall measured stator current

$$\underline{v}^{\mathrm{hx}}(s) = \begin{bmatrix} K_{\mathrm{pd}} + K_{\mathrm{id}}\dfrac{1}{s} & -\omega(6n+1)K_{\mathrm{zq}}\dfrac{1}{s} \\ \omega(6n+1)K_{\mathrm{zd}}\dfrac{1}{s} & K_{\mathrm{pq}} + K_{\mathrm{iq}}\dfrac{1}{s} \end{bmatrix} \cdot \underline{e}^{\mathrm{hx}}(s) + \begin{bmatrix} -\tilde{K}_{\mathrm{pd}} & \dfrac{\omega(6n-1)}{(s+j\omega 12n)}\tilde{K}_{\mathrm{zq}} \\ \dfrac{\omega(6n-1)}{(s+j\omega 12n)}\tilde{K}_{\mathrm{zd}} & \tilde{K}_{\mathrm{pq}} \end{bmatrix} \cdot \underline{e}^{\mathrm{hx}}(s+j\omega 12n) \tag{9}$$

$$K_{\mathrm{id}} = \frac{R}{T_{\mathrm{d}x}}, \quad K_{\mathrm{pd}} = K_{\mathrm{zd}} = \frac{L_{\mathrm{m}}}{T_{\mathrm{d}x}}, \quad \tilde{K}_{\mathrm{pd}} = \tilde{K}_{\mathrm{zd}} = \frac{L_{\Delta}}{T_{\mathrm{d}x}}, \quad K_{\mathrm{iq}} = \frac{R}{T_{\mathrm{q}x}}, \quad K_{\mathrm{pq}} = K_{\mathrm{zq}} = \frac{L_{\mathrm{m}}}{T_{\mathrm{q}x}}, \quad \tilde{K}_{\mathrm{pq}} = \tilde{K}_{\mathrm{zq}} = \frac{L_{\Delta}}{T_{\mathrm{q}x}} \tag{10}$$

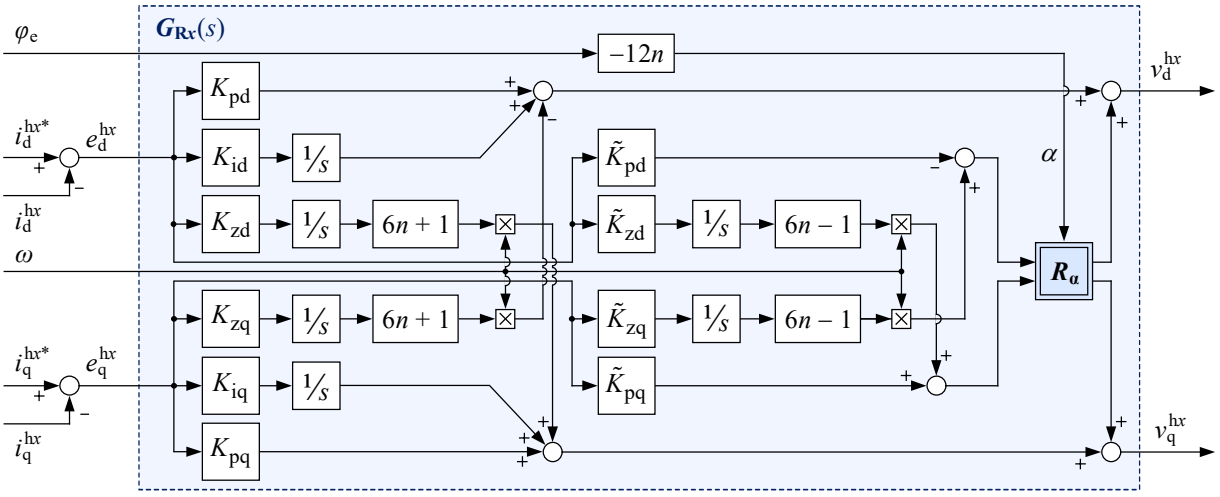

Fig. 3. Continuous-time implementation of the proposed current controller (9) for a single harmonic.

vector $\underline{i}_{\mathrm{abc}}$ as actual value. For the calculations, the measured actual stator current vector is transformed into each controller's reference frame by a DQ transformation that is adapted to the harmonic order by multiplying the actual rotor angle φ_{e} with the order x of the regarded harmonic. The resulting transformation angle is $\theta_x = x\varphi_{\mathrm{e}}$. The Eqs. (11) and (12) describe the adapted transformations.

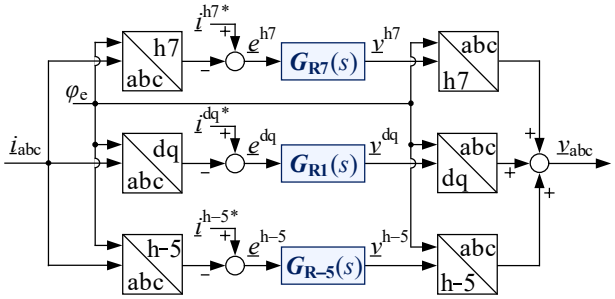

Fig. 4. Combination of the fundamental and multiple harmonic current controllers.

$$\underline{i}^{\mathrm{h}x} = \frac{2}{3}\begin{bmatrix} \cos(\theta_x) & \cos\left(\theta_x - \frac{2\pi}{3}\right) & \cos\left(\theta_x - \frac{4\pi}{3}\right) \\ -\sin(\theta_x) & -\sin\left(\theta_x - \frac{2\pi}{3}\right) & -\sin\left(\theta_x - \frac{4\pi}{3}\right) \end{bmatrix} \cdot \underline{i}_{\mathrm{abc}} \quad (11)$$

$$\underline{v}_{\mathrm{abc}} = \begin{bmatrix} \cos(\theta_x) & -\sin(\theta_x) \\ \cos\left(\theta_x - \frac{2\pi}{3}\right) & -\sin\left(\theta_x - \frac{2\pi}{3}\right) \\ \cos\left(\theta_x - \frac{4\pi}{3}\right) & -\sin\left(\theta_x - \frac{4\pi}{3}\right) \end{bmatrix} \cdot \underline{v}^{\mathrm{h}x} \quad (12)$$

The time constants $T_{\mathrm{d}x}$ and $T_{\mathrm{q}x}$ of the individual controllers define their bandwidths. For large time constants, the controllers only react on their selective harmonic. For small time constants, the controllers also respond to adjacent harmonics and start to interact with the other controllers. E.g. the controller for the 7th harmonic shows the strongest interference with the fundamental controller and the 13th harmonic controller. The disturbing influence of the other controllers causes a deviation of the dynamic behavior from the desired characteristic, but does not cause an error in steady state. Since the absolute difference between the harmonic frequencies is enlarged with increasing speed, the interaction between the individual controllers is reduced. The selection of the time constants should be adapted to the required speed and dynamic range of the application. To enable a dynamic torque control while minimizing the interaction of the harmonic controllers, the fundamental controller is tuned five times faster than the harmonic controllers for the simulations and measurements in this paper. The direct and quadrature components of the individual controllers are implemented with equal time constants.

IV. Simulative Validation

The proposed controller is used for the current control of a PMaSynRM. A machine model with rotor angle and current dependent parameters is used for the simulative validation. The inductances and the PM-flux are based on look-up-tables generated by FEM simulations and contain harmonics up to the 90th order. The direct and quadrature inductances given in Tb. I are averaged values over the rotor angle for $i_{\mathrm{d}}^{\mathrm{dq}} = i_{\mathrm{q}}^{\mathrm{dq}} = 0\,\mathrm{A}$. The regarded PMaSynRM has distributed windings, which leads to a good attenuation of the low order harmonics. Hence, the -17th and 19th harmonics are dominant.

TABLE I
Parameters of the PMaSynRM (Y-connected) and the control system for the simulations and measurements

Symbol	Meaning	Value
R	Stator winding resistance	0.7 Ω
L_{d}	Direct inductance	8.8 mH
L_{q}	Quadrature inductance	49.9 mH
Ψ_{PM}	Permanent magnet flux	103 mWb
$\hat{i}_{\mathrm{max}}$	Max. stator current amplitude	50 A
p	Number of pole pairs	2
V_{DC}	Applied DC-voltage	500 V
f_{PMW}	Switching frequency	10 kHz
$T_{\mathrm{d1}}, T_{\mathrm{q1}}$	Time constants of the fundamental current control	2 ms
$T_{\mathrm{d}x}, T_{\mathrm{q}x}$	Time constants of the harmonic current control	10 ms

First, the elimination of the harmonics is examined. 10 HCs $n = \{\pm 1, \pm 2, \pm 3, \pm 4, \pm 5\}$ are used in parallel to eliminate current harmonics up to the 31st harmonic. The machine is operated at 1000 rpm and the fundamental controller is set to $i_{\mathrm{d}}^{\mathrm{dq}*} = -10\,\mathrm{A}$ and $i_{\mathrm{q}}^{\mathrm{dq}*} = 10\,\mathrm{A}$ before the HCs are activated. The setpoint currents of all HCs are set to zero to eliminate the current harmonics. Figure 5 shows the phase currents and voltages in the stationary abc-reference frame for the activation of the HCs at t = 0 s. In addition, the amplitudes of the voltage and current harmonics before and after the activation of the harmonic current controllers are listed in Tb. II.

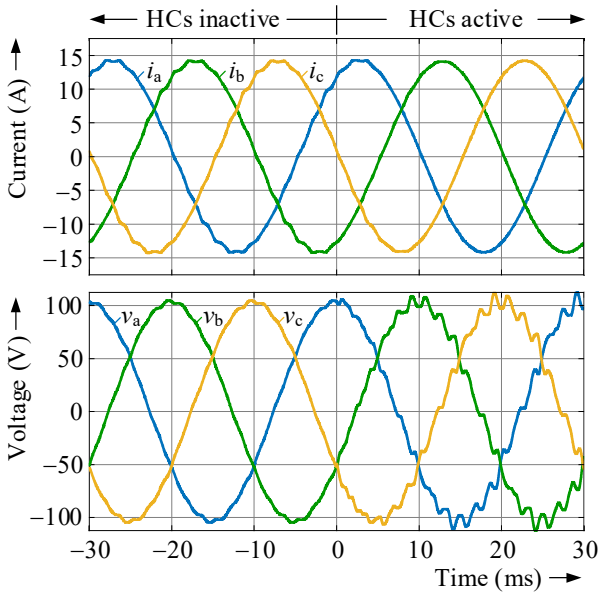

Fig. 5. Simulated phase currents and voltages during the activation of the harmonic controllers (1000 rpm).

The small deviations from ideally sinusoidal voltage waveforms in the lower diagram, before the HCs are activated, show that the fundamental controller already reacts on the current harmonics but is not able to eliminate them. When the HCs are activated, the amplitudes of the voltage harmonics strongly increase and the current harmonics are almost perfectly eliminated within a fundamental electrical period. Table II shows that harmonics above the 31st are not eliminated.

TABLE II
AMPLITUDES OF VOLTAGE AND CURRENT HARMONICS FOR ACTIVE AND INACTIVE HARMONIC CONTROLLERS (SIMULATION)

Harmonic order h	Current amplitude		Voltage amplitude	
	Inactive HCs	Active HCs	Inactive HCs	Active HCs
1	14.14 A	14.14 A	103.5 V	103.5 V
-5	18.6 mA	< 0.1 mA	51.5 mV	640.7 mV
7	55.0 mA	< 0.1 mA	14.6 mV	1609.0 mV
-11	17.1 mA	< 0.1 mA	20.5 mV	432.4 mV
13	16.0 mA	< 0.1 mA	21.0 mV	448.2 mV
-17	171.8 mA	< 0.1 mA	221.9 mV	6906.0 mV
19	132.1 mA	< 0.1 mA	50.7 mV	1325.0 mV
-23	30.0 mA	< 0.1 mA	47.9 mV	2057.0 mV
25	18.9 mA	< 0.1 mA	10.1 mV	580.2 mV
-29	5.8 mA	< 0.1 mA	12.5 mV	697.9 mV
31	2.3 mA	< 0.1 mA	6.5 mV	399.5 mV
-35	21.9 mA	17.9 mA	27.9 mV	675.9 mV
37	18.7 mA	15.9 mA	16.0 mV	536.9 mV
-41	1.8 mA	1.2 mA	5.3 mV	74.1 mV
43	1.9 mA	2.2 mA	5.4 mV	72.9 mV

The injection of current harmonics is suitable to compare the dynamic characteristic between the proposed novel controller in the HRF and the resonant implemented RINV controller. Exemplary, the injection of the -5th harmonic is tested at 1000 rpm. The simulated controller in the HRF corresponds to the combination given in Fig. 4 and is implemented for the time constants listed in Tb. I. The quadrature element of the setpoint current for the -5th harmonic $i_{\mathrm{q}}^{\mathrm{h}-5*}$ changes abruptly from 0 A to 5 A. To show the current waveforms without superpositions, the reference value for the fundamental currents is set to zero. The resulting phase currents are displayed in the upper plot of Fig. 6.

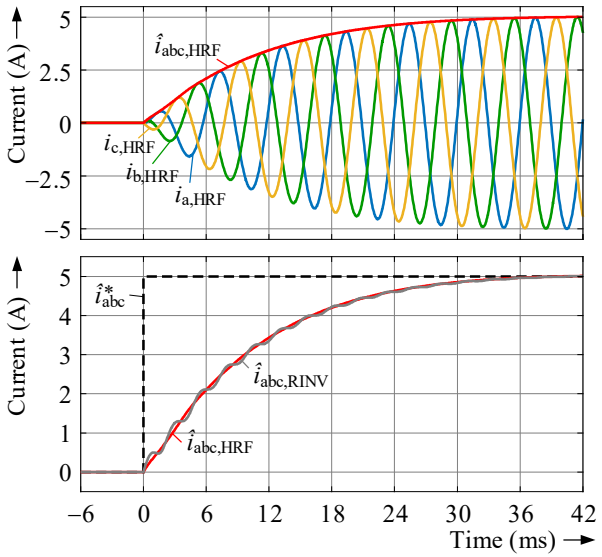

Fig. 6. Simulated phase currents for the injection of the -5th harmonic with proposed HC in HRF and RINV controller (1000 rpm).

Additionally, the actual stator current amplitude $\hat{i}_{\mathrm{abc,HRF}}$ is drawn in red. $\hat{i}_{\mathrm{abc,HRF}}$ follows the desired PT1 characteristic (7) nearly perfect. Small deviations are caused by the interaction of the parallel controllers, since no filters are implemented. Note that fundamental currents other than zero, will not change the dynamic behavior. The lower plot in Fig. 6 compares the stator current amplitude of the proposed controller with that of the resonant implementation (denoted by $\hat{i}_{\mathrm{abc,RINV}}$). The compared resonant controller is implemented for the ±6th harmonic in the fundamental dq-reference frame (= 7th and -5th harmonic in abc-reference frame), as proposed in [6], with the same time constant as the proposed controller in the HRF. In steady state, both controllers result in the same current waveforms. However, the resonant implemented controller clearly shows a greater oscillation during the transient phase. The RINV controller simultaneously controls the -5th and 7th harmonics. The setpoint value for the -5th harmonic acts as disturbance for the 7th harmonic control, causing the oscillation with the 12th harmonic order, recognizable in Fig. 6. The proposed novel controller (9) avoids this effect, since the -5th and 7th harmonics are controlled independently with individual setpoint vectors.

V. EXPERIMENTAL VALIDATION

For the experimental validation, the proposed controller is implemented on a rapid-prototyping system (dSpace MicroLabBox) to control the currents of the real PMaSynRM. The controller structure (Eq. (9) / Fig. 3) is transformed into the discrete-time frequency domain using the bilinear transformation (13) to consider the discrete-time operation of the control system.

$$s \triangleq \frac{2}{T_s} \cdot \frac{z-1}{z+1} = 2 \cdot f_{\mathrm{PWM}} \cdot \frac{z-1}{z+1} \tag{13}$$

T_s denotes the sample time of the rapid-prototyping system and z represents the discrete-time frequency variable. For resonant controller implementations, the time-discretization can lead to pole displacements that require additional correction measures, see [7]. Since the relevant harmonic appears as DC value for the implementation of the controller in the HRF, these effects do not appear. Hence, only the phase shift of the output voltage caused by the delay of the control system should be considered.

To compensate this delay, the phase angle for the back-transformation of the voltage from the x^{th} HRF into the abc-reference frame should be corrected [8]. Within this work, good results were achieved, if the delay of half a sampling period is compensated. The angles α of the rotation $\boldsymbol{R}_{\boldsymbol{\alpha}}$ within the individual HC and θ_x of the back-transformation Eq. (12) have to be modified according to Eq. (14).

$$\alpha = -12n \cdot \left(\varphi_{\mathrm{e}} + \omega \frac{T_{\mathrm{s}}}{2}\right), \quad \theta_x = x \cdot \left(\varphi_{\mathrm{e}} + \omega \frac{T_{\mathrm{s}}}{2}\right) \tag{14}$$

The HCs are implemented up to the 31st order, the

realized time constants are equal to the simulations. The speed control of the asynchronous machine, which is used as load, is also implemented on the MicroLabBox.

To validate the elimination of the current harmonics, the activation of the HCs is regarded for the same operating point that was simulated in Fig. 5. The measured phase currents and voltages are shown in Fig. 7. The amplitudes of the individual harmonics for active and inactive HCs are calculated by a fast Fourier transformation and listed in Tb. III. Since the three phase currents/voltages are not perfectly symmetrical, the listed amplitudes are the average of the amplitudes of the individual phases.

TABLE III
AMPLITUDES OF VOLTAGE AND CURRENT HARMONICS FOR ACTIVE AND INACTIVE HARMONIC CONTROLLERS (MEASUREMENT)

Harmonic order h	Current amplitude		Voltage amplitude	
	Inactive HCs	Active HCs	Inactive HCs	Active HCs
1	14.14 A	14.14 A	102.3 V	102.6 V
-5	31.8 mA	6.2 mA	45.7 mV	419.6 mV
7	18.3 mA	3.3 mA	37.1 mV	198.6 mV
-11	7.7 mA	2.0 mA	8.9 mV	108.2 mV
13	10.8 mA	2.3 mA	14.6 mV	270.4 mV
-17	255.4 mA	2.0 mA	349.9 mV	8610.0 mV
19	171.9 mA	3.3 mA	131.1 mV	958.3 mV
-23	32.7 mA	1.7 mA	47.3 mV	1786.0 mV
25	19.7 mA	1.4 mA	12.3 mV	433.7 mV
-29	10.8 mA	1.4 mA	17.4 mV	804.8 mV
31	6.6 mA	2.7 mA	6.3 mV	458.1 mV
-35	26.1 mA	41.4 mA	48.9 mV	1618.0 mV
37	11.8 mA	19.7 mA	18.6 mV	694.8 mV
-41	3.4 mA	7.2 mA	6.4 mV	327.9 mV
43	2.0 mA	4.9 mA	4.4 mV	259.7 mV

The dominant harmonics of the real machine are slightly bigger than the ones of the simulation model, but the general behavior is equal. The harmonic controllers are able to reduce the dominant -17th current harmonic from >250 mA to only 2 mA. The remaining amplitudes of the controlled current harmonics are as big as the inaccuracy of the current sensors. Hence, a better elimination is not achievable.

In addition, the stability of the proposed control system for fundamental current variations, respectively torque variations, and speed variations is demonstrated. The setpoint of the fundamental direct current i_d^{dq*} is changed abruptly from -5 A to -10 A, while the machine is operated at 1000 rpm with $i_q^{dq*} = 10\,\text{A}$. The measured fundamental direct current is shown in Fig. 8 a) for inactive HCs and in Fig. 8 b) for active HCs. The comparison between the plots a) and b) show that the harmonic controllers do not significantly deteriorate the dynamic characteristic or the stability of the fundamental controller. Instead, the elimination of the 19th and -17th harmonics, that appear as ±18th harmonic in the fundamental dq-reference frame, can clearly be seen. The not ideal PT1 characteristic is caused by deviations between the parameters used for the controller design and the real machine parameters.

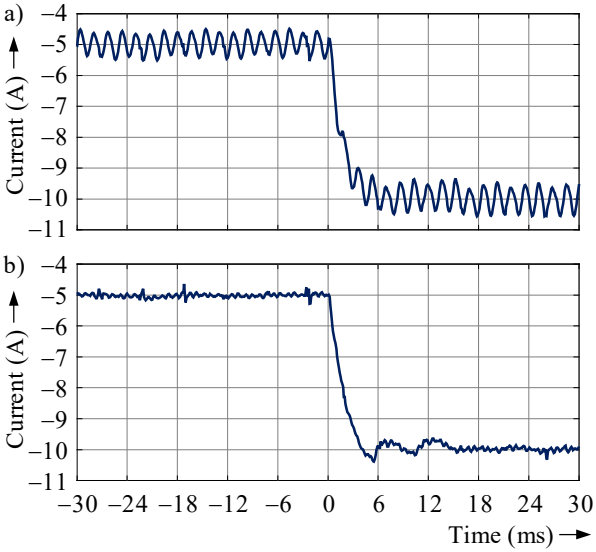

Fig. 8. Measured fundamental d-current for a step of the setpoint value a) without HCs and b) with HCs (1000 rpm).

To proof the stability during speed and therewith frequency variations, the beginning of an acceleration process is regarded in Fig. 9. The maximum acceleration achievable by the load machine on the test bench is

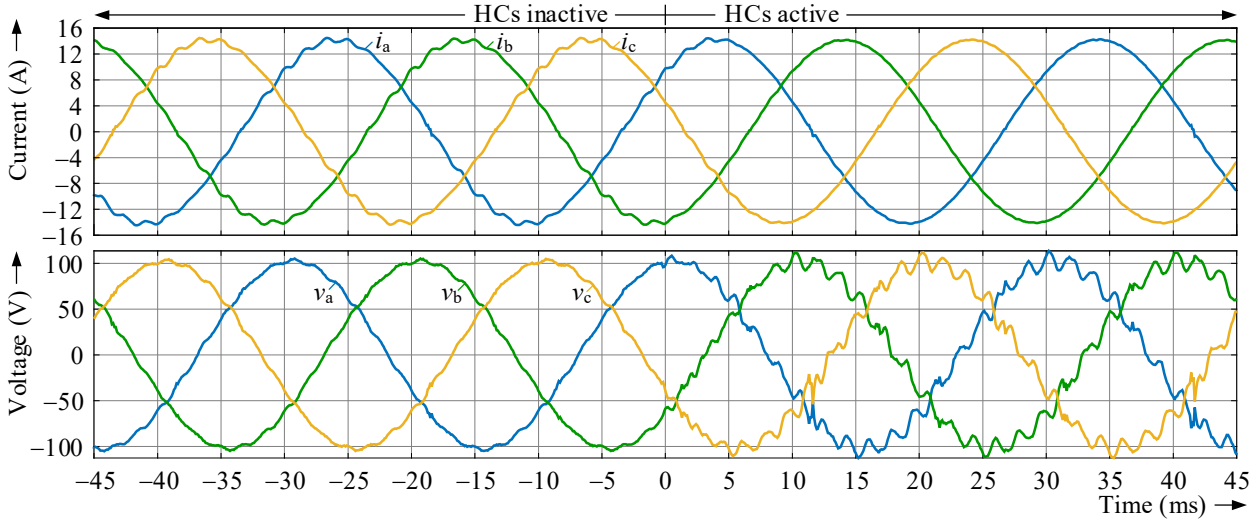

Fig. 7. Measured phase currents and voltages during the activation of the harmonic controllers (1000 rpm).

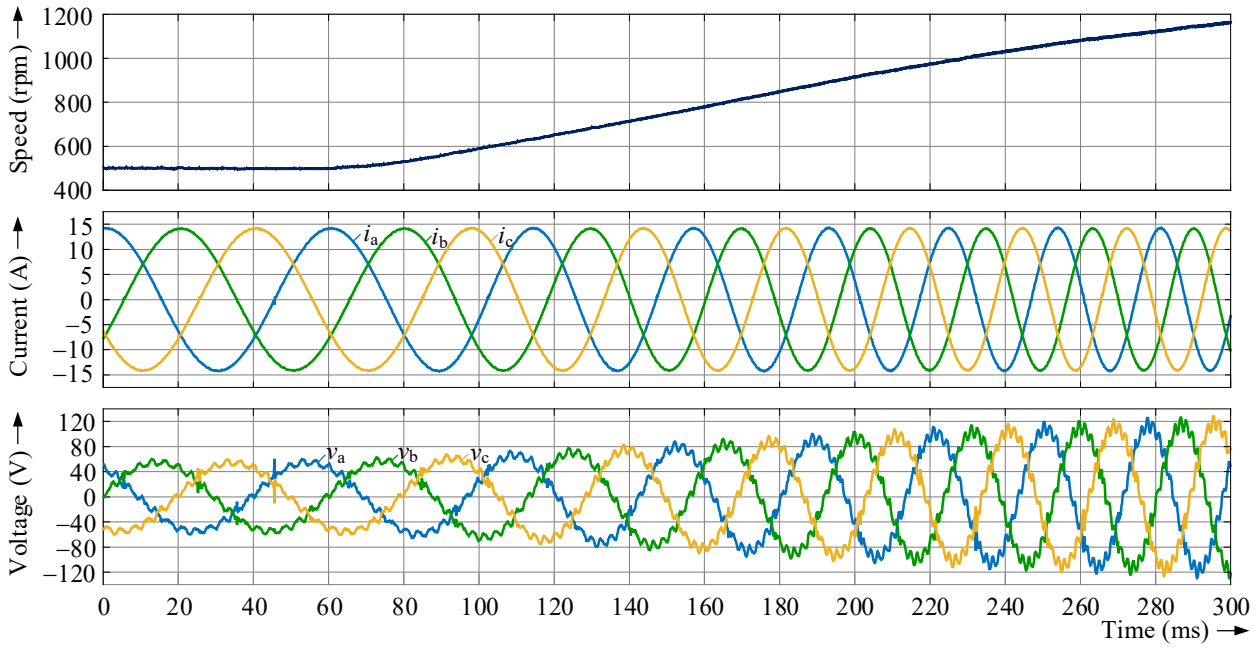

Fig. 9. Measured speed, phase currents and voltages during an acceleration ($i_d^{dq*} = -10\,A$, $i_q^{dq*} = 10\,A$).

approximately 3000 rpm/s. Through the implementation in the HRFs, the relevant harmonic always appears as DC measure in the HCs, regardless of the speed. Hence, the very good elimination of the current harmonics is not deteriorated during the speed variation.

However, the test bench measurements have shown an upper speed limit for the use of the HCs, caused by the limitations of the inverter. Since the output voltage is only updated discretely in time with the switching frequency, the waveform of the output voltage deviates more from the desired sinusoidal shape for increasing frequencies. Hence, for high speeds and high orders of the controlled harmonics, the inverter is not able to actually provide the output voltage waveform desired by the controller. As consequence, the HCs cannot control the harmonics sufficiently anymore and can become instable. On the test bench, it was empirically determined that less than six PWM periods per period of the highest controlled harmonic can lead to instable behavior. The maximum speed n_{max}, at which a sufficient elimination of the harmonics is achieved on the test bench, can be approximated by Eq. (15), depending on the maximum controlled harmonic order h_{max}.

$$n_{max} \approx \frac{60\frac{s}{min} \cdot f_{PWM}}{p \cdot h_{max} \cdot 6} \tag{15}$$

The use of the 31st harmonic controller is stable up to approx. 1600 rpm. The dominant 19th harmonic can be eliminated up to 2600 rpm. Figure 10 shows the measured phase currents and voltages for the operation of the machine in field weakening at 2500 rpm with $i_d^{dq*} = -21\,A$, $i_q^{dq*} = 7\,A$. The HCs up to the 19th order are activated, higher order HCs are inactive. At this speed, the output frequency of the 19th HC is already 1583 Hz.

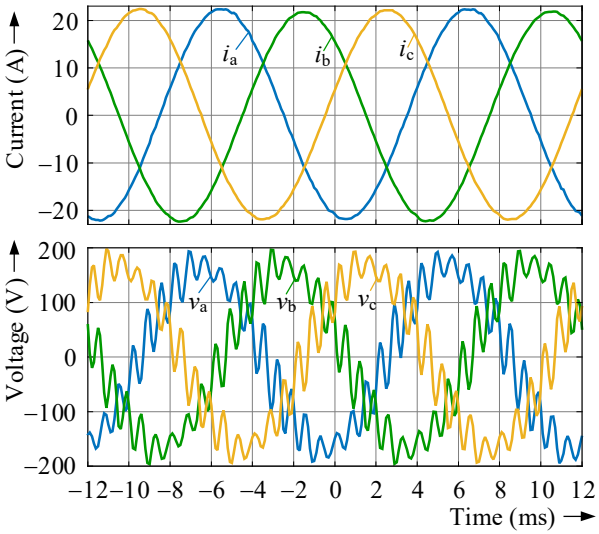

Fig. 10. Measured phase currents and voltages for high frequencies (2500 rpm, $i_d^{dq*} = -21\,A$, $i_q^{dq*} = 7\,A$, up to 19th HC active).

If the speed is further increased, the highest order active HC will start to disturb the current control and lead to additional distortion of the current waveform. Therefore, the individual HCs should be turned off for speeds greater than the limit formulated by Eq. (15).

Without claiming general validity, it should be mentioned that the proposed controllers, implemented in the HRF, have shown higher speed stability on the test bench than the resonant RINV controllers. The RINV controller for the same harmonic order has already led to instabilities at an approx. 20 % lower speed. The effect of the instability was also more severe. Although the current control is distorted above the maximum speed given by Eq. (15) when using the HRF controllers, the fundamental wave is still kept at its desired value. In contrast, with the RINV controllers, an increasing oscillation occurred that

triggered the inverter's overcurrent shutdown.

With the given test bench setup, an optimization of the torque ripple due to selective harmonics injection cannot be confirmed reliably, so far. The torque measuring shaft of the test bench does not allow to distinguish whether the DUT machine or the load machine causes the measured torque variation. Since the measured torque shows an dominant 6th harmonic, which does not fit to the observed current harmonics of the PMaSynRM, the author suspects the asynchronous load machine as the source of the disturbance.

Nevertheless, a first approach to smoothen the torque by selective harmonic injection is presented in Fig. 11. The upper plot shows the phase currents, while the measured torque is given in the lower plot. For $t < 0$ ms, the harmonic controllers are inactive and the peak-to-peak torque ripple is approx. 2.5 Nm. At $t = 0$ ms, the HCs are activated. In contrast to the measurements presented so far, the setpoint currents of the harmonic controllers are no longer set to zero, but to empirically determined values. It can be seen, that the total harmonic distortion of the phase currents is increased after the activation of the HCs. However, the measured peak-to-peak torque ripple is reduced to approx. 1.4 Nm. For this measurement, the -5th, 7th, -17th and 19th current harmonic are injected with up to 600 mA to influence the 6th and 18th torque harmonic.

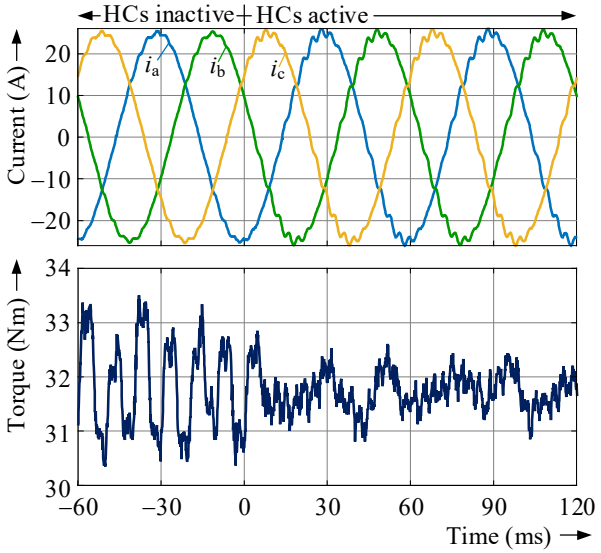

Fig. 11. Measured phase currents and torque before and after the injection of selective harmonics (500 rpm, $i_d^{dq*} = -20\,\text{A}$, $i_q^{dq*} = 15\,\text{A}$).

VI. Conclusions

This paper analytically derives the transfer characteristic of anisotropic synchronous machines in harmonic reference frames that rotate with integer multiples of the fundamental electrical angular frequency. It is shown, that the excitation with a single voltage harmonic results in two superimposed current harmonics. Based on this transfer characteristic, an inverse plant based controller structure for the implementation in the harmonic reference frame is presented. The calculation of the controller coefficients, the combination of several harmonic controllers and the required measures for a discrete-time implementation are provided. Simulations and measurements on the test bench validate the desired stationary and dynamic behavior of the novel controller. The proposed harmonic controller concept enables an elimination of the controlled harmonics, even during speed or torque variations. The upper frequency limit for the use of the HC is defined by the switching frequency of the inverter.

Compared to resonant controller implementations, the implementation in the HRFs allows a more selective and therefore slightly more robust system response on individual harmonics. Hence, the proposed controller could realize a stable control of the harmonics on the test bench for significantly higher speeds than the compared resonant implementation. On principle, the reduction of torque pulsations due to an injection of selective current harmonics is also confirmed by the proposed controller.

References

[1] T. M. Jahns and W. L. Soong, "Pulsating torque minimization techniques for permanent magnet AC motor drives-a review" in IEEE Transactions on Industrial Electronics, vol. 43, no. 2, pp. 321-330, April 1996, doi: 10.1109/41.491356.

[2] N. Nakao and K. Akatsu, "Suppressing Pulsating Torques: Torque Ripple Control for Synchronous Motors" in IEEE Industry Applications Magazine, vol. 20, no. 6, pp. 33-44, Nov.-Dec. 2014, doi: 10.1109/MIAS.2013.2288383.

[3] Weidong Zhu, B. Fahimi and S. Pekarek, "A field reconstruction method for optimal excitation of permanent magnet synchronous machines" in IEEE Transactions on Energy Conversion, vol. 21, no. 2, pp. 305-313, June 2006.

[4] M. Seilmeier, S. Arenz, B. Piepenbreier and I. Hahn, "Model based closed loop control scheme for compensation of harmonic currents in PM-synchronous machines" SPEEDAM 2010, 2010, pp. 1-6, doi: 10.1109/SPEEDAM.2010.5542398.

[5] Y. Okajima and K. Akatsu, "Harmonic current control for Interior Permanent Magnet Synchronous Machines applying current controller design method by using complex vectors" IECON 2016 - 42nd Annual Conference of the IEEE Industrial Electronics Society, 2016, pp. 2815-2820, doi: 10.1109/IECON.2016.7793428.

[6] J. Karttunen, S. Kallio, J. Honkanen, P. Peltoniemi, P. Silventoinen, “Stability and performance of current harmonic controllers for multiphase PMSMs” in Control Engineering Practice,Volume 65, 2017, pp. 59-69.

[7] A. G. Yepes, F. D. Freijedo, J. Doval-Gandoy, O. Lopez, J. Malvar and P. Fernandez-Comesaña, "On the discrete-time implementation of resonant controllers for active power filters," 2009 35th Annual Conference of IEEE Industrial Electronics, Porto, Portugal, 2009, pp. 3686-3691, doi: 10.1109/IECON.2009.5415136.

[8] Bojoi, R., Limongi, L.R., Profumo, F., Roiu, D. and Tenconi, A. (2009), Analysis of current controllers for active power filters using selective harmonic compensation schemes. IEEJ Trans Elec Electron Eng, 4: 139-157. https://doi.org/10.1002/tee.20392.